POLYMER SOLUTION INJECTION ANALYSIS IN THE POROUS MEDIA

Rodrigo Amaral Minamisawa, amaral.ro@gmail.com
Rosângela Barros Zanoni Lopes Moreno, zanoni@dep.fem.unicamp.br
Department of Petroleum Engineer – State University of Campinas - UNICAMP

Abstract.

The injection of viscous water induced by the addition of polymer in a porous media has the purpose of modifying the mobility rate between the displaced and displacing fluids viscosities. This provides a better sweep efficiency, thus reducing the water production while increasing the petroleum recovery.
This method has been intensively described in the literature, showing distintive results. In general, these works report laboratory experiments where a polymer is injected on porous media reservoir or representatives samples. In this context, the present article aims to compare the tests results of water and viscous water (produced by HPAM) injection on the oil recovering.
Firstly, the stability criteria of Rapoport&Leas as well as the graphic area of flow stability was defined, assuring the viscous strength predominance over the capillarity and gravitational forces on the porous media flow. Once determinated the constant flow, two imbibitions and two draining were performed. During the tests, the pressures along the sample were measured, providing the effective permeabilities, the relative permeability curves, and the saturation bank displacement, among others.
As a result, the resistance factor (mobility reduction) and residual resistance factor (permeability reduction) were determined, the water and oil production curves were compared and the recovery and sweep efficiency factor defined.

Keywords*: EOR, Polymer flooding, Tests criteria, Laboratory Tests, Relative Permeability, Fractionary Flow*

1. INTRODUCTION

Chemical methods for oil recovery such as the viscosified water injection by polymer addition for enhancement of sweep efficiency have been demonstrated as economically viable in several projects in Brazil and abroad. Poellitzer *et. al.*, 2009, and Wang *et. al.*, 2009 have shown successful cases in Austria and China. Also, Mello *et. al.*, 2010, have reported a reevaluation of the field of Carmópolis, Buracica and Canto do Amaro in Brazil, places where the technology could be potentially applied.

Recently, several companies presented their oil field production projects using viscosified water injection, showing a set of data of Brazilian fields such as Peregrino, Campo do Siri and Papa Terra. Associated to results obtained in the literature, these experiments allowed the determination of selection criteria necessary for process applications.

The selection criteria known as "*screening*" are rules that reveal a variation range for oil and reservoir parameters that allow the application of different processes (LAKE, 1989, SORBIE, 1991 and GREEN&WILLHITE, 1998). These criteria were widely discussed in the literature as mentioned before, and consider variables such as oil API degree, absolute permeability and oil viscosity among others.

It is important to highlight that these works do not provide data of the investigated fields, which makes the reproducibility of the results often unpractical. Also, in respect to the selection of attributes, the study of significant parameters related to the displaced and displacing fluids becomes fundamental because of their interaction with the porous media.

The optimization injection process starts with the definition of the optimized method through the criteria analysis. The viscosified water injection aims to increase the areal sweep efficiency (E_A) when compared with the water injection. This can be explained by the mobility rate (M) change. Figure 1 shows the sweep efficiency in function of the mobility rate (for a *five spot*), where one can verify that the left displacement of M increases as decreasing the E_A (Figure 1).

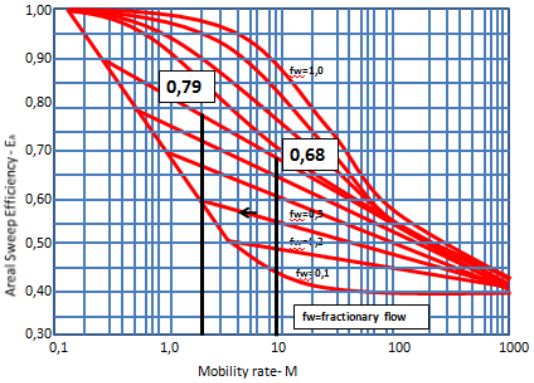

Figure 1. Sweep efficiency by mobility rate (*Five-spot* case – adapted from ROSA et. al., 2006)

The mobility rate relation, which is the ratio between the displacing fluid mobility (λ_D) behind the saturation front and the displaced fluid mobility (λ_O) on its bank is shown in Equation 1. One can see that a reduction of the injected fluid viscosity or an increase of the relative permeability are the only parameters susceptible to changes. Theoretically, the relative permeability is independent of the fluid viscosity, i.e., only a change in viscosity results in the reduction of M.

$$\mathbf{M} = \frac{\lambda_D}{\lambda_O} = \frac{K_W}{\mu_W}\frac{\mu_O}{K_O} \tag{1}$$

Where K is the relative permeability and μ the viscosity, "w" and "o" the index for water and oil.

Therefore, the displacing fluid viscosity is an essential term for increasing the sweep efficiency. Looking at the fluid customization, it is possible to establish a relation between the fluid viscosity and its concentration, which allows a post correlation with E_A. Figure 2 shows the injection fluid viscosity in relation to the solution concentration for different shear rates.

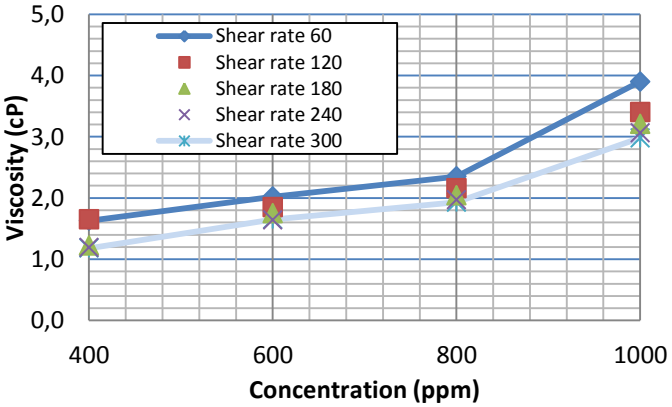

Figure 2. Injection fluid viscosity by HPAM concentration

In this work, a comparison between the impact of water and viscosified water injection on the sweep efficiency, recovery factor and water production parameters analysis is presented. An injection fluid customization method will also be presented, linking the concentration of the polymer solution to the increase of sweep efficiency, as demonstrated.

2. METODOLOGY

Sandstone "Botucatu" was selected for the flooding laboratory tests (the rock is widely described by GOMES et. al., 1996). The samples were collected using a drilling machine and its dimensions and weight measured. Later, the core was inserted in a coreholder and the gas porosity and absolute permeability were measured (Figure 3 – Table 1).

Figure 3. Botucatu Sandstone, weight, coreholder insert, Porosimeter and Permeabilimeter.

Table 1. Core dimensions, weight, porosity and permeability.

Dimension	Diameter (cm)	Lenght (cm)	Weight (g)	Porosity (%)	Gas Absolute Permeability (mD)
Value	3,71	32,50	775,66	33,05	7089

Following, the saturation of the porous media was obtained using a mix of water and NaI (150K ppm). At the same time, the displacing and displaced fluids parameters were determined in a Rheometer and a Densimeter (Table 2).

Table 2. Fluids viscosity and density

Fluid	Water solution with NaI(1)	Nujol oil(1)	Viscosified water with NaI(1)
Viscosity (cP)	0,99	120	1,6
Density (g/ml)	1,142	0,862	1,142

(1): measured at 23°C

The Rheometer measurements provided the shear stress in function of the shear rate, and the viscosity in function of the shear rate for the viscosified water fluid (Figure 4a and 4b – zoom at the work range). The results show that the viscosity value is approximately 1.6 with Newtonian behavior. The high values of shear stress seen in figure 4a are due to the equipment inertia for short shear rates and turbulent flow for long shear rates (over 100 sec^{-1}).

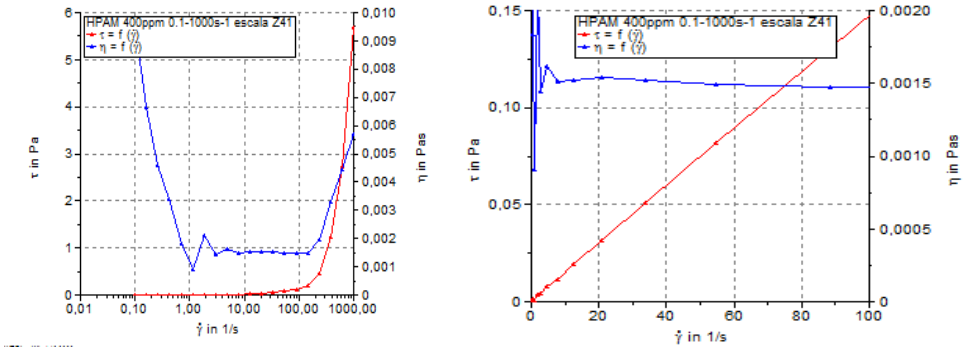

Figure 4a and 4b. Shear Stress by Shear rate and Viscosity by Shear rate.

The collected data allowed the utilization of the similarity tests criteria and the operational limits such as dimensionless numbers reported by Gomes, 1997 and Santos *et. al.*, 1997. Both authors have defined dimensionless numbers assuring the viscous strength predominance over the capillarity and gravitational forces on the porous media flow. Also, some parameters for precisions pressure and water cut measurements, sample representativity and two parameters that guarantees the convective flow over the diffusive one and the thermodynamic equilibrium of the multiphase system (Eq. 2, 3, 4, 5, 6, 7, 8, 9).

$$N_c = \frac{U\mu_o}{\sigma} < \frac{\sqrt{k\phi}}{R} \quad (2)$$

$$\varepsilon_c = \frac{\sigma\sqrt{k\phi}}{\mu_o LU} \ll 1 \quad (3)$$

$$\varepsilon_g = \frac{(\rho_w - \rho_o) g 2rkk_{ro}^o}{UL\mu_o} \ll 1 \quad (4)$$

$$\varepsilon_p = \frac{\Delta p^*}{\Delta p}, UL \gg \frac{kk_{ro}^o}{\mu_w}\Delta p^* \quad (5)$$

$$U\Delta t^* \ll \alpha L \quad (6)$$

$$\varepsilon_w = \frac{\Omega_*}{U\pi R^2 \phi \Delta t^*} \ll 1 \quad (7)$$

$$\varepsilon_D = \frac{D}{LU} \ll 1 \quad (8)$$

$$\varepsilon_\tau = \frac{\tau^* U}{\phi L} \ll 1 \quad (9)$$

Here: N_c Capillary Number, "g" gravitational acceleration, "k" absolute permeability, k_{ro} oil relative permeability, "L" core length, "r" core radius, "R" capillary radius, ρ_w water specific weight, ρ_o oil specific weight, μ_o oil visocsity, μ_w water viscosity, ô shear rate, ô* delay time, Δp minimum pressure drop, $å_c$ capillary viscous rate, $å_D$ Schimidt´s number, $å_g$ gravity viscous rate, $å_p$ sample representativity criterion, $å_w$ water cut criterion, $å_{ô}$ delay number, Ù* minimum sample volume, U flow speed, D diffusion coefficient, á ratio between the sample volume and the pore volume and ϕ porosity.

Graphically, the dimensionless numbers results show an optimal work window correlating the core length with the flow velocity for water and viscosified water flooding cases (Figures 5a and 5b). This workspace allows the flow limits determination for the core length.

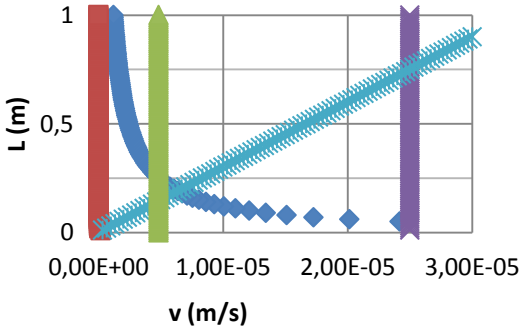

Figura 5a. Waterflood admissible area.

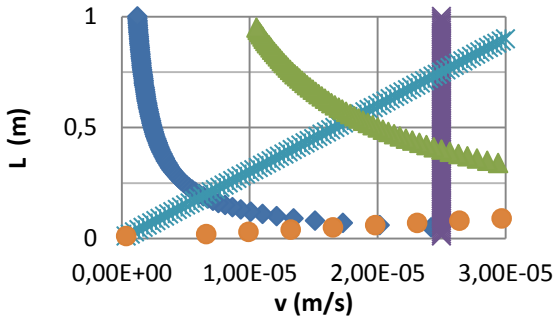

Figura 5b. Viscosified water flood admissible area.

After analyzing the curves, a flow velocity of 0.000016 m/s was determined, corresponding to 1 cc/min of flow rate. The tests protocol used, including all the flooding process (imbibitions, drainages and polymer injection) can be seen on Figure 6. One can see that during the tests, the pressure along the core (with some 320 psi transducers), and the injected/produced fluids weight were achieved.

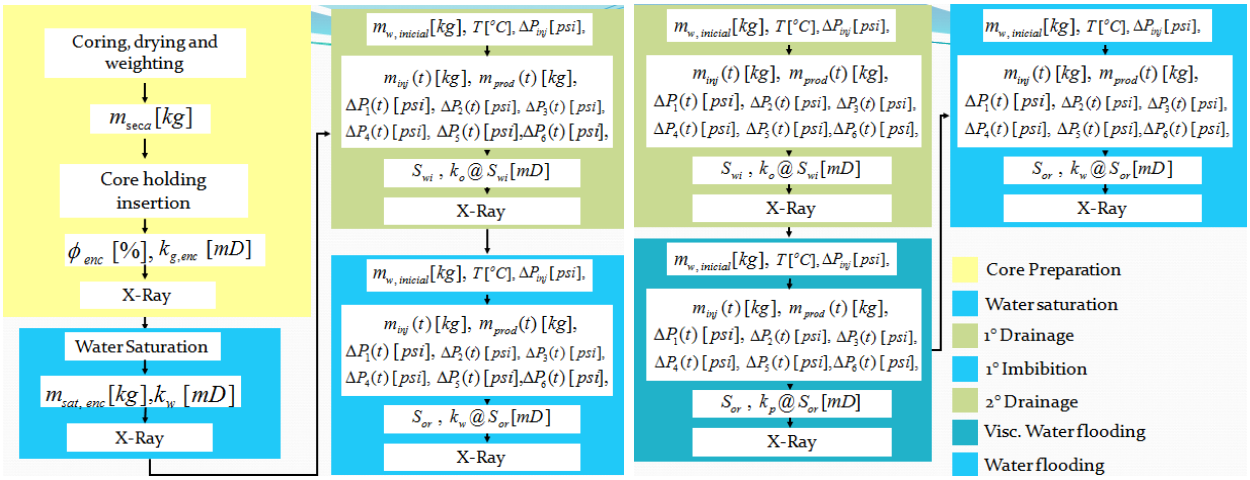

Figure 6. Tests protocol: 1° Imbibition, 1° Drainage, 2° Imbibition, 2° Drainage, Visosified water injection, water flooding.

The second imbibition was the water flooding. The second drainage is aimed to convert the core for its initial conditions in terms of water and oil saturation. This process allows a later comparison between the water and viscosified water flooding. In the end of each stage, the terminal points of saturation and effective permeabilities were determined (Table 3).

Table 3. Effective permeabilities for water, oil and viscosified water flooding.

Parameters	Values (mD)	Saturation (%)
Water absolute permeability ($k_{w@Sw=100\%}$)	5.246	S_{wi}^{1E}=100
Oil effective permeability ($k_o@S_{wi}^{1D}$)	5.538	S_{wi}^{1D}=10,70
Water effective permeability ($k_{w@Sor}^{2E}$)	466	S_{or}^{2E}=34,21
Oil effective permeability ($k_o@S_{wi}^{2D}$)	6.106	S_{wi}^{2D}=9,81
Viscosified Water effective permeability ($k_{p@Sor}^{3E}$)	181	S_{or}^{3E}=20,49

The water and oil production data collected after the *breakthrough* were used to plot the relative permeabilities and fractionary flow curves (Figure 7 and 8). The relative permeabilities curves were determined through the non-permanent method described by Honarpour, 1986. Welge, 1952 (apud HONARPOUR, 1986), as shown in Equation10:

$$S_{w,av} - S_{w2} = f_{o2} Q_w \tag{10}$$

Here: $S_{w,av}$ is the average water saturation, S_{w2} is the produced water saturation, Q_w is the water cumulative flow rate and f_{o2} is the produced oil fraction.

And:

$$f_{o2} = \frac{q_o}{q_o + q_w} \tag{11}$$

Here: q_o is the produced oil flow rate and q_w the water one.

Combined with Darcy´s law, both 10 and 11 equations take the following form:

$$f_o = \frac{1}{1 + \frac{k_w \mu_o}{\mu_w k_o}} \tag{12}$$

The equations derived for the individual phase relative permeabilities from unsteady- state method can be seen on Equation 13 and 14. This method is known as JBN method because it is an extension of Welge´s work made by Johnson, 1959 (apud HONARPOUR, 1986).

$$K_{ro} = \frac{f_{o2}}{d\left(\frac{1}{Q_w I_r}\right)/d\left(\frac{1}{Q_w}\right)} \tag{13}$$

And:

$$K_{rw} = \frac{f_{w2}}{f_{o2}} \frac{\mu_w}{\mu_o} k_{ro} \tag{14}$$

Where I_r, the relative injectivity, is defined on equation 15:

$$I_r = \frac{total\ injectivity}{initial\ injectivity} = \frac{(q_w/\Delta p)}{(q_w/\Delta p)_{initial}} \tag{15}$$

The conditions for the JBN method application its necessary that:

- The core be homogeneous.
- The pressure gradient be large enough to minimize capillary pressure effects
- The pressure differential across the core be sufficiently small compared with total operating pressure so that compressibility effects are insignificant.
- The driving force and fluid properties be held constant during the tests.

The curves can be seen on Figures 7.

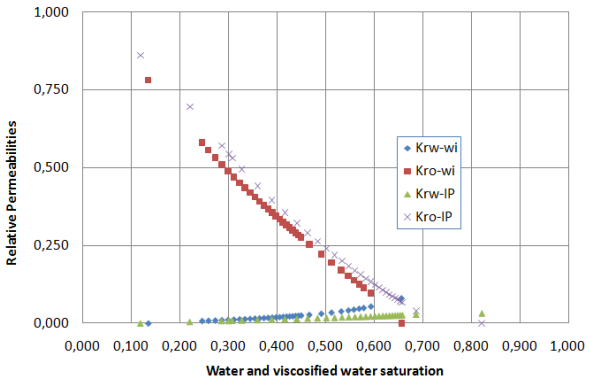

Figure 7. Relative permeabilities on water (wi) and viscosified water flooding (IP).

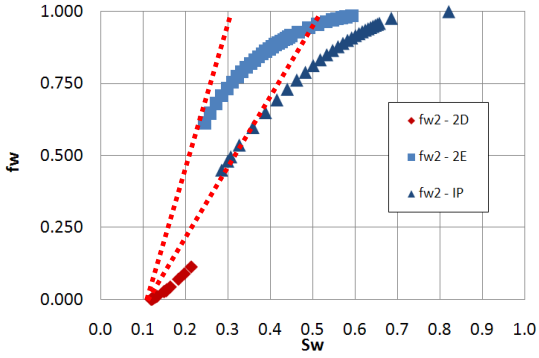

Figure 8. Fractionary flow on water (2D), oil (2E) and viscosified water flooding (IP).

Figure 7 shows the relative permeabilities for water and viscosified water flooding, where one can see that the porous media is water wet.

Rosa, 2006, reported that the relative permeability curves should be overlapped once it is not correlated to the viscosity of the fluids. However this is not observed because the rock used in this experiment is wet in different levels by distinct fluids. A down level of the curve indicates that the viscosified water prone to flow near the pore wall as well as occupy the smaller diameter pores.

Figure 8 indicates that the average water saturation behind the front saturation are 31.5% and 50%. This shows that in the moment of *breakthrough*, the water saturation on the porous media is higher for the injected viscosified water case, consequently there is less remaining oil, therefore resulting in superior oil recovery.

This phenomenon can be explained by the relative permeability reduction, fact that can be observed on Figure 7. Because of the smaller viscosified water mobility, it is more difficult to flow in the porous media leading to a better oil displacement.

Such front saturation advance was demonstrated through X-Ray measurements. The mathematical analysis implicit were described by Gomes, 1997, starting with the Beer law´s for the total attenuation coefficient (Equation 16).

$$I = I_o e^{-\Psi x^*} \tag{16}$$

Here: Io the intensity of the incident X-Ray wave, I is the intensity of the outgoing wave, x the core thickness and Ψ the coefficient of total linear attenuation.

With the coefficient of total linear attenuation defined, the attenuation coefficient for the saturated core with fluid *I* can be determined (Equation 17)

$$\Psi_{Ri} = (1 - \emptyset)\Psi_M + \Psi_i \emptyset \tag{17}$$

Where Ψ_{Ri} is the core saturated with fluid *i* coefficient of linear attenuation, $\emptyset$ the porosity, Ψ_M the core coefficient of linear attenuation and Ψ_i the fluid *i* coefficient of linear attenuation.

This method still provides the porosity determination (Equation 18), if the core be saturated with more than one fluid.

$$\emptyset = \frac{(\Psi_{Ri} - \Psi_{Rj})}{(\Psi_i - \Psi_j)} \tag{18}$$

The Equations 18 still take forms (Equation 19, 20 and 21) providing the saturation calculus (Equation 22)

$$S_1 + S_2 = 1 \tag{19}$$

$$\Psi_{R1} = (1 - \emptyset)\Psi_M + \Psi_1 \emptyset \tag{20}$$

$$\Psi_{R2} = (1 - \emptyset)\Psi_M + (\Psi_1 S_1 + \Psi_2 S_2)\emptyset \tag{21}$$

$$S_2 = \frac{(\Psi_{R1} - \Psi_{R2})}{\emptyset(\Psi_1 - \Psi_2)} \tag{22}$$

Where: Ψ_{R1} is the core saturated with fluid *1* coefficient of linear attenuation and Ψ_{R2} is the core saturated with fluid *2* coefficient of linear attenuation.

3. RESULTS

Following the proposed customization model described, the results at first show a reduction of the mobility rate (table 2 and 3) from 10.09 to 2.22 on the presented flooding cases. The values, when inserted on the Figure 1, supply an increase of the areal sweep efficiency of 11%, approximately. Such phenomenon can be still overviewed in other curves and analysis as mass flow vs. injection time, water (W_p) and oil (N_p) production per injected porous volume (VPI) and recovery factor (Fr) vs. VPI.

The *breakthrough* postponement can be seen on the mass flow per injection time graph (Figure 9). One can see that the viscosified water injection is delayed in about 24 minutes. The constant injection flow rate of 1cc/min can be also observed (injection curves wi and IP) as well as a step on the water produced curve (wi), related to the multiphase flow (water/oil).

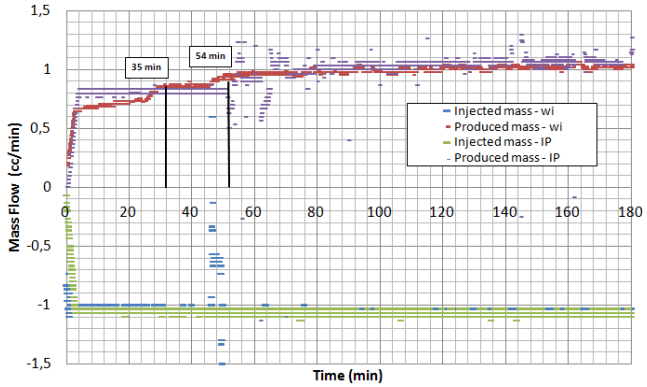

Figure 9. Mass flow of produced/injection water, oil and viscosified water per time

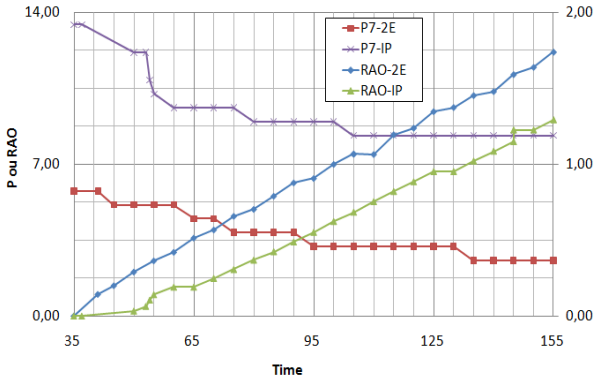

Figure 10. RAO and pressure for water/viscosified water cases per normalized time.

The *breakthrough* delay on the viscosified case presented on Figure 9 indicates a decrease of the water production. This phenomenon can be seen on Figure 10 (RAO) which correlates the water/oil ratio per normalized time. On the same curve it is possible to identify a reduction of about 23% in RAO for 2.8 VPI.

Concerning to the sweep efficiency increase, Figure 11 shows anticipation of the oil production. The rise of the curve on the viscosified water flooding case (Np – IP) makes clear this behavior when compared with the water injection one (Np). The postponed *breakthrough* can be identified too, once the curve related to the water production (Wp) moves to the right (viscosified water production – HPAM).

It is important to note that the overlap occurrence of the oil production curves before the *breakthrough*, which indicates similar conditions for both flooding cases.

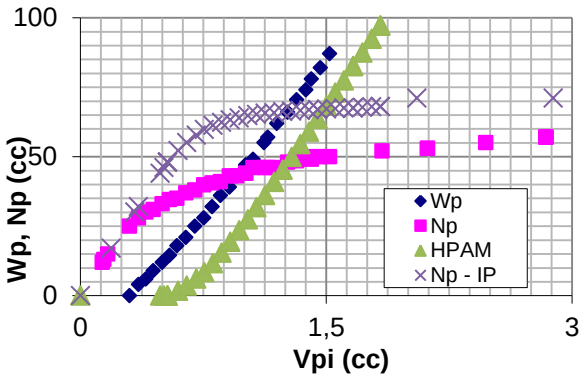

Figure 11. Water, oil and viscosified water productions curves.

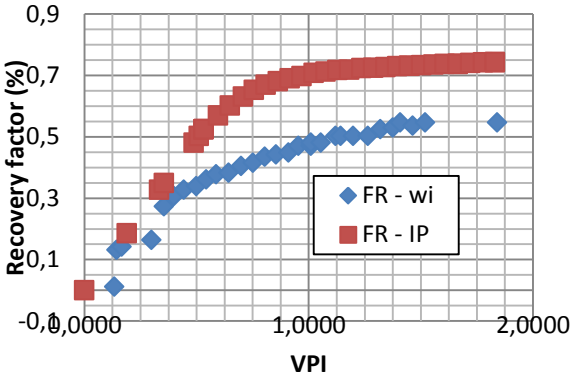

Figure 12. Recovery factor for water (wi) and viscosified water (IP) flooding cases per VPI.

Green&Willhite, 1998 define total bulk displacement as the ratio between the volume of oil displaced by the volume of oil *in place*. These parameters known as recovery factor (Fr) when plotted by VPI can be seen on Figure 12. A higher level of the viscosified case (FR-IP) is observed, fact that indicates an oil production anticipation in the process. The parameter increases 20% approximately after 2 VPI.

The pressures acquired during the process along the core length (transducers installed on the beginning of the core and every 1 inch the first three, every 2 inches the consecutive two and the last one 10 cm far from the injection face). The results were plotted and can be seen on Figure 13a, 13b and 14 for water, viscosified water and the last continuous water flooding respectively.

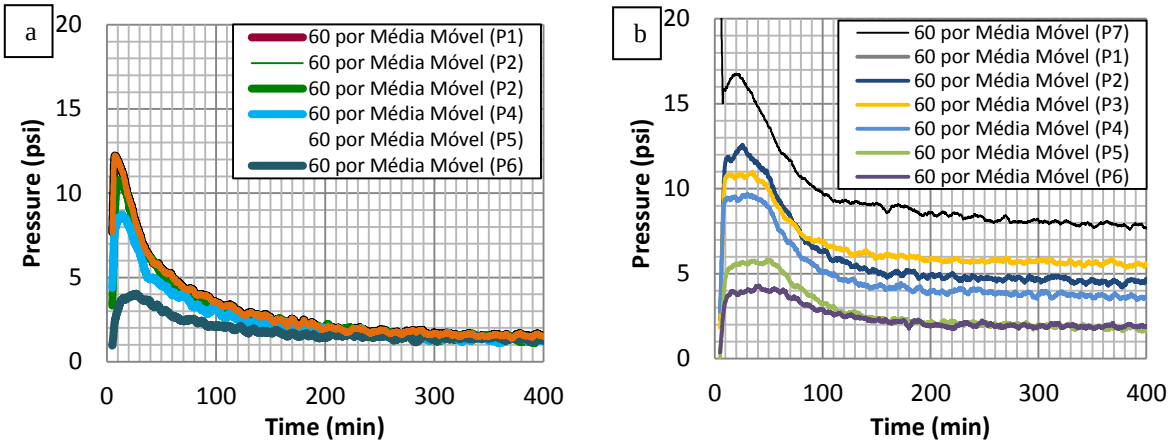

Figure 13. Pressure along the core for the water (a) and viscosified water (b) flooding cases per time.

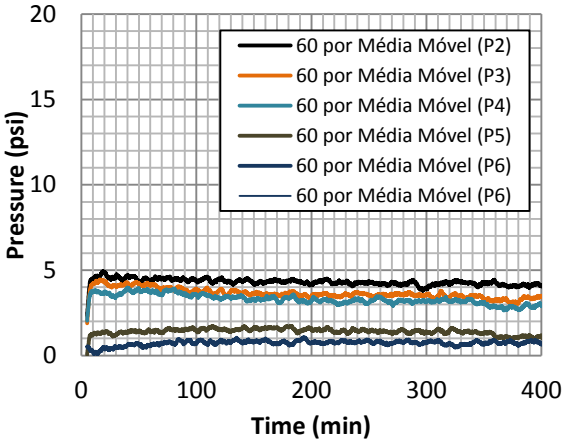

Figure 14. Pressure along the core for the water flooding case (after the viscosified fluid injection) per time

The Figures 13a and 13b show an increase on the injection pressure of the viscosified water flooding over the water injection when compared all the measurements. The first transducer on the injection core face presents an increase from 12.5 to 16.5 psi, indicating a higher resistance for the polymeric solution flow, behavior that is usually related to some absorbance effects (literature).

Therefore, the absorbance can explain the relative permeability reduction shown on the Figure 7, ensuring that this parameter is not related to the viscosity as described by Rosa, 2006.

Rômulo, 2005, after some laboratory tests experiments correlated the polymer solution absorbance on the porous media with the adsorbance of light by collecting some samples of produced fluid (in his case water and viscosified water flooding) and analyzing them in a spectrophotometer. These data were still related to a reduction of mobility and permeability described by Baijal, 1982, who presents the resistance factor (FR – Equation 23) and residual resistance factor (FRR – Equation 24). According to both authors, the measured pressures can be used to calculate the mobility and permeability reduction.

The mobility reduction is referred to the increase of the fluid viscosity and can be observed on the Equation 23.

$$FR = \frac{\lambda_w}{\lambda_p} = \frac{k_w}{\mu_w} \cdot \frac{\mu_p}{k_p} = \left(\frac{\Delta P}{L \cdot \bar{v}}\right)_p / \left(\frac{\bar{v} \cdot L}{\Delta P}\right)_w = \frac{\Delta P_p}{\Delta P_w} \tag{23}$$

Here: λ is the mobility, *k* the relative permeability, μ the viscosity, ΔP the pressure gradient, L the length, $\bar{v}$ the flow velocity and "*w*" and "*p*" the index for water and viscosified water, respectively.

Beyond the mobility reduction, the porous media relative permeability decrease can also be seen. This phenomenon can also be calculated by the use of the pressures ratio, however using the data from the first water flooding and the last one (after the viscosified water injection). The residual resistance factor (equation 24) shows this behavior.

$$FRR = \frac{\Delta P_{w1}}{\Delta P_{w2}} \tag{24}$$

Here: ΔP is the pressure gradient and 1 and 2 the water flow before and after the viscosified water application.

In the present work the FR is 2,10 and FRR, 1,83, using the pressures acquired on the transducer 1, placed 1 inch of distance from the injection core face. Usually these values are compared with the same data from another kind of polymer and correlated to the spectrophotometer data. Unfortunately, this work presents only HPAM polymer tests and the fluid samples collected had some oil (that was inside the core and were produced after the *breakthrough*) fluid that probably interfered in the light diffraction of the referred equipment.

The last parameter analyzed was the X-Ray data. Figure 15 shows the saturation of oil/water per core length where one can see the Buckley&Leverett, 1942, flow behavior for the drainages (oil injection), known as *piston with leak* (Figures 15 – 1D and 2D). For the water injection (1E after 13 min) it is not possible to identify some change on the curve shape, only a raise of the water saturation level. This can indicate the occurrence of *fingering* effects. Nevertheless, the viscosified water graph (Pol after 27min and Pol after 37min) shows an inclined curve prone to the *piston with leak* model described.

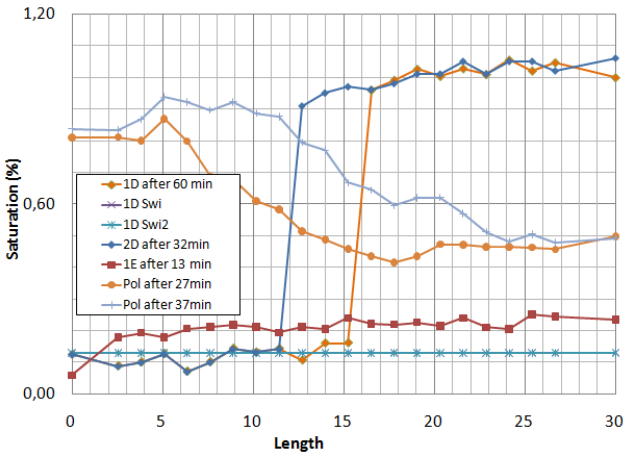

Figure 15. Saturation per core length

4. CONCLUSIONS

The present work compares the water and viscosified water flooding on the enhanced oil recovery. Countless previous tests were made looking for the equipments calibration as well as the parameters determination as flow rate, for example, which allowed the correct application of such technology.

Firstly it was determined the *screening* through the literature values for absolute permeability, oil API, among others. Afterwards began the tests criterion definitions using the Rapoport&Leas dimensionless numbers added to others (apud Santos, 1997). It was identified that under low flow rates there was *piston with leak* displacement for the water injection, showing almost no difference when used the viscosified water. On the other hand, under high flow rates the water *breakthrough* happened quickly, showing *fingering* effects (the Reynolds number calculation for this case showed turbulent flow too).

As soon as the flow rate was defined, the transducer used had to be determined. So, the Darcy´s law could be applied, but carefully, since the porous media response for the viscosified fluids flow was not so linear.

The absolute permeability was another fundamental parameter to be analyzed even after the *screening* selection. It was verified, for example, that low values (<100mD) turned the transducers reading not viable beyond the problem of the Buckley&Leveret displacement occurrence on the water injection case.

Looking for the fluids characterization, the Rheometer was very useful correlating different polymer solutions concentration to their viscosity, so as to allow the definition of the best content value to be injected.

The X-Ray equipment also show very good results, but it is important to note the necessity of doing many acquisitions during the imbibitions and drainages and to adjust the saturations levels by mass balance. On this matter, it was made one acquisition every 12 minutes (time to reset the equipment).

After the previous test and the determination of all the reported parameters, the tests began. So, a high absolute permeability core of 32,5cm was chosen (7.09 D) and a flow rate of 1,00cc/min, which guaranteed the viscous strenght forces predominance over the capillary and gravitational ones.

Consequently it was observed an increase of 11% on the recovery factor, an oil anticipation production and the reduction on the RAO of 23% (2,8VPI) approximately. The saturation curves acquired by X-Ray and mass balance method makes it clear the sweep efficiency increase and the S_{or} decrease, which validates the fluid customization method proposed.

For future tests it is recommendable the absorbance determination of different viscosified fluids concentrations on the porous media. This data can be obtained through the injection of different concentration solutions on cores with similar absolute permeability.

The absorbance (referring to relative permeability) per viscosified water concentration, added to the sweep efficiency per mobility ratio relations, can be useful to create a numerical model which correlates sweep efficiency per viscosified water concentration.

The collect data can still be used to feed a numerical simulator, and so to generate a real field case. Being, thus, an indispensable tool for the industry.

5. ACKNOWLEDGEMENTS

Many thanks to Prof. Euclides Joset Bonet, Luiz B. Pompeu Neto and Leandro A. Fernandes for the laboratory tests discussions and support.

6. BIBLIOGRAPH

Baijal, S.K. **Flow Behavior of Polymers in Porous Media**. Tulsa, Oklahoma: PennWell Publishing Company, 1982.

Buckley, S. E., Leverett, M. C., **Mechanism of Fluid Displacement in Sands**. *Trans.* AIME, 146, 1942.

Green, D.W; Willhite, G. P. **Enhanced Oil Recovery.** Richardson: Henry L. Doherty Fund, 1998.

Gomes, J. A. T, Tibana, P., Correa, A. C. F.; **Análise Petrográfica e Petrofísica dos arenitos Botucatu**, Conexpo Arpel, Rio de Janeiro, 1996.

Gomes, J. A. T, **Visualização e Análise do Deslocamento Imiscível e Instável em Meio Poroso Consolidado.** Tese de Doutorado, Departamento de Ciência e Engenharia de Petróleo, Universidade Estadual de Campinas, 1997.

Honarpour, M., L. Koederitz, and A. H. Harvey, **Relative *Permeability* of Petroleum Reservoirs**, 143 pp., CRC, Boca Raton, Fla., *1986.*

Lake, L. W. **Enhanced Oil Recovery**, New Jersey: Prentice Hall, 1989.

Melo, M.A., Silva I.P.G., Mezzomo, R.F., Lima, J.C., Aguiar, A.A., **Sustainability Evaluation of Polymer Pilots For Petroleum Recovery in Brazil**, Rio Oil&Gas Expo&Conference, Rio de Janeiro, RJ, 2010.

Poellitzer S., Floriant T., Clemens T., **Revitalising a Medium Viscous Oil Field by Polymer Injection, Pirawarth Field, Austria.** SPE 120991, 2009

Romulo, A., T., **Reologia e Teste de Deslocamento de Soluções Poliméricas com Potencial de Uso em Recuperação Avançada de Petróleo.** Dissertação de Mestrado, Departamento de Engenharia e Arquitetura, Universidade de Salvador, 2005.

Rosa, A. J., Carvalho, R. S., Xavier, J.A.D., **Engenharia de Reservatórios de Petróleo**, Editora Interciência, 2006.

Santos, R. L. A., Bedrikovetsky, P., Holleben, C. R., **Optimal Design and Planning for Laboratory Corefloods.** Latin American and Caribbean Petroleum Engineering Conference and Exhibition, Rio de Janeiro, SPE 39038, 1997.

Sorbie, D P. K. S. **Polymer- Improved Oil Recovery,** Boca Raton: CRC Press Inc., 1991.

Wang, D., Dong, H., LV, C., Fu, X., & Nie, J. **Review of practical experience of polymer flooding at Daqingg**. *SPE Reservoir Evaluation and Engineering, 12*(3), 470-476, 2009.

7. RESPONSIBILITY NOTICE

The authors are the only responsible for the printed material included in this paper.